# NATIONAL INSTITUTE FOR FUSION SCIENCE

Band Rejection Filter for Measurement
of Electron Cyclotron Emission
during Electron Cyclotron Heating

M. Iwase, K. Ohkubo, S. Kubo and H. Idei

(Received - Sep. 8, 1995 )

## RESEARCH REPORT
## NIFS Series

NAGOYA, JAPAN

# Band Rejection Filter for Measurement of Electron Cyclotron Emission during Electron Cyclotron Heating

IWASE Makoto, OHKUBO Kunizo*, KUBO Shin*, IDEI Hiroshi*

Department of Fusion Science,

The Graduate University for Advanced Studies,

Chikusa-ku, Nagoya, 464-01, Japan

* National Institute for Fusion Science, Chikusa-ku, Nagoya, 464-01, Japan

## Abstract

For the measurement of electron cyclotron emission from the high temperature plasma, a band rejection filter in the range of 40~60 GHz is designed to reject the 53.2 GHz signal with large amplitude from the gyrotron for the purpose of plasma electron heating. The filter developed with ten sets of three quarters-wavelength coupled by $TE_{111}$ mode of tunable resonant cavity has rejection of 50 dB and 3 dB bandwidth of 500 MHz. The modified model of Tschebysheff type for the prediction of rejection is proposed. It is confirmed that the measured rejection as a function of frequency agrees well with the experimental results for small coupling hole, and also clarified that the rejection ratio increases for the large coupling hole.

KEYWORDS : electron cyclotron emission, electron cyclotron heating, cavity, band rejection filter, Tschebysheff

# 1 Introduction

For the conventional diagnostics of the electron temperature of high temperature plasmas, electron cyclotron emission (ECE) in the range of millimeter wave has been measured with a multi-channel radiometer system. To heat plasma electrons, the electron cyclotron heating (ECH) at the fundamental frequency and higher harmonics as the simplest method has been carried out in the toroidal magnetic confinement devices. In the compact helical system (CHS), the millimeter wave from the 53.2 GHz gyrotron with 100 kW of power produces the plasma by the second harmonic ECH. A horn antenna connected to the radiometer in the frequency range of 40~60 GHz picks up the 53.2 GHz signal from the gyrotron as a stray with the level as high as the local oscillator in the radiometer. The normalized bandwidth of the gyrotron oscillation is around $10^{-6}$. To observe the second harmonic ECE from all the regions of the plasma during the second harmonic ECH, a rejection filter with the narrow band and the high attenuation is required, since the ECE just near the ECH frequency is especially important. The development of such kind of the filter is also essential in the application of the collective ion Thomson scattering.

In Wendelstein-7 AS, the band rejection filter at 70 GHz has been used for the fundamental ECE measurement during ECH [1,2]. It consists of a piece of straight E-band waveguide and five cylindrical cavities, which are spaced by three-quarter wavelength in the waveguide. The waveguide is aligned perpendicular to the axis of the cylindrical cavity. The transverse magnetic field component of the fundamental waveguide mode is coupled to the longitudinal magnetic field in the cavity by a hole in the waveguide side wall. The diameter of the coupling hole is 1.7 mm that is determined experimentally. In this case, to get the high $Q$ value, the coupling mode in the cavity is chosen to be $TE_{011}$ mode.

2

As this mode is not the fundamental mode of the cylindrical cavity, spurious resonances may occur. To study the propagation of heat wave by ECH in CHS by means of ECE, we have developed series of three quarter-wavelength coupled resonant cavity. The typical design method for a band rejection filter which is a quarter wavelength coupled resonant cavity is well known as a Tschebyscheff type [3]. By introducing an inductance and a capacitance in the resonant circuit, the rejection characteristics is calculated from the Tschebyscheff polynomial. It is necessary to satisfy a specific attenuation value and band width at the resonant frequency of the filter in the ECE measurement during ECH. To compare experimental results with theoretical ones, we take the finite ohmic loss in the cavity and the frequency-dependence on the waveguide between cavities into consideration. The method extended from the traditional design method of a Tschebysheff type is also applicable for the band pass filter.

The paper consists of five sections. The aspect of the filter design is described in section 2. Experimental results are given in section 3. In section 4, the results applied to the full band width 40~60 GHz for the ECE diagnostics are described. Conclusions are given in section 5.

# 2   Design of the band rejection filter

A band rejection filter with the $U$-band rectangular waveguide (4.8 mm × 2.4 mm) is developed for easy insertion in the radiometer. Here, we take a tunable frequency and adjustable attenuation and a narrow bandwidth determined by $Q$ value in resonant circuit into consideration. The schematic drawing of the filter is shown in Fig. 1. A waveguide made by cutting an aluminium block and the aluminium plate with ten coupling holes of

which interval is 5.3 mm are prepared. The interval is equal to the $3\lambda_g/4$ at 53.2 GHz. Here, $\lambda_g$ is the wavelength in the waveguide. On all the holes the tunable resonant cavities are connected.

## 2.1 $Q$ value of cylindrical cavity

The unloaded $Q$ value $Q_0$ of $TE_{mn1}$ mode [4] determined by the dimension of the cylindrical cavity at the frequency $\omega_0/2\pi$ is given by

$$Q_0 = \frac{[\chi_{mn}^2 - m^2][\chi_{mn}^2 + (\pi D_{cav}/2l_{cav})^2]^{3/2}}{2\pi[\chi_{mn}^4 + \pi^2\chi_{mn}^2 D_{cav}^3/4l_{cav}^3 + (\pi m D_{cav}/2l_{cav})^2(1 - D_{cav}/l_{cav})]}\frac{\lambda_0}{\delta} . \quad (1)$$

$$\lambda_0 = D_{cav}/\sqrt{(\chi_{mn}/\pi)^2 + (D_{cav}/2l_{cav})^2} , \quad (2)$$

where $D_{cav}$ and $l_{cav}$ are the diameter and the length of the cavity, and $\delta = \sqrt{2/\omega\mu_0\sigma}$ and $\lambda_0$ are the skin depth and the wavelength in free space, respectively. Here, $\mu_0$ is the permeability in vacuum and $\sigma$ is the conductivity of the wall material. The value of $\chi_{mn}$ is the n-th root in derivative of Bessel function $J'_m(\chi)$ and is 1.8411 for $TE_{11}$ mode. To maximize $Q_0$, $D_{cav}$ and $l_{cav}$ are selected to be 4.0 mm and 5.0 mm, respectively. The length of cavity is adjusted by movable tuning plunger. The calculated $Q_0$ of the aluminium cavity is 4120.

The attenuation factor $\alpha$ between the waveguide and the cylindrical cavity [4] is given by

$$\alpha = 10^{-1.6\sqrt{1-(1.7d/\lambda_0)^2}(t/d)} . \quad (3)$$

where $d$ and $t$ are the diameter and the thickness of the cavity hole, respectively. The aluminium plates with various sizes of $d = 1.4, 1.6, 1.8, 2.0$ and 2.4 mm with $t = 0.4$ mm are prepared. To couple with the $B_x$ and $B_z$ components in the $U$-band waveguide, the position of coupling holes is deviated from the central line. The configuration of holes is

4

shown in Fig. 2. The coupling of $TE_{10}$ mode in the $L$-band waveguide with $TE_{11}$ mode in the cylindrical cavity by the magnetic field is examined in Appendix I. The external $Q$ value $Q_E$ with coupling hole of $d = 2.0$ mm is calculated to be 7730. It should be noted that $Q_E$ is proportional to $d^{-6}$ (see appendix I).

## 2.2 Equivalent circuit

In order to analyze the performance of the band rejection (or pass) filter such as the Tschebyscheff type, equivalent circuit [4] including an inductance $L$ and a capacitance $C$ as resonant circuit was used. Here, the coupling of the waveguide with the cavity is treated with an ideal transformer model with the turn ratio $n$. However, it is not sufficient to estimate the transmission property of the band rejection filter by only $L$ and $C$, because ohmic losses are not negligible in the range of the millimeter wave. It is noteworthy especially that the total ohmic loss relates with the value of an attenuation at the resonant frequency. Introducing the resonant cavity of a resistance $R$ spaced by the arbitrary length $\ell$ into the consideration as shown in Fig. 3, we modify the conventional design of Tschebysscheff type filter. The frequency dependence of the multi-band rejection filter with $N$ cavities is discussed in terms of parameters of $Q_0$ , $R$ and $n$. The impedance $Z_{cav}$ [4] and resonant frequency $\omega_0/2\pi$ of single resonant circuit are given by

$$Z_{cav} = \frac{n^2 R}{1 + j\Delta\omega Q_0/\omega_0} = \frac{n_R Z_0}{1 + j\Delta\omega Q_0/\omega_0} . \tag{4}$$

$$\omega_0 = 1/\sqrt{LC} . \tag{5}$$

Here, the $Q_0$ value (that is defined as $\omega_0 RC$) is the unloaded $Q$ value of the resonator and $n_R = n^2 R/Z_0$. The value of $\Delta\omega$ (that is defined as $\omega - \omega_0$) is a deviation from the resonant frequency. As shown in Fig. 3, the band rejection filter is composed of many sets

5

of the resonant cavity and transmission. Here, the susceptance $jB_{hol}$ due to the coupling hole [5] is neglected. In analysis for wide band we include $jB_{hol}$ as discussed in Appendix II.

The $F$-matrix of this system as shown in Figs. 3, 4 are expressed as

$$[F] = [F_0][F_{hol}][F_{cav}][F_{wg}][F_{hol}][F_{cav}][F_{wg}] \cdots ,$$

$$\cdots [F_{hol}][F_{cav}][F_{wg}][F_{hol}][F_{cav}] = \begin{pmatrix} A & B \\ C & D \end{pmatrix} , \tag{6}$$

where $[F_0]$, $[F_{hol}]$, $[F_{cav}]$ and $[F_{wg}]$ are the $F$-matrices for the element of the generator, the scattering from the coupling hole, the cavity and the waveguide between adjacent cavities, respectively. The matrices of $[F_0]$, $[F_{hol}]$, $[F_{cav}]$ and $[F_{wg}]$ are given [5] by

$$[F_0] = \begin{pmatrix} 1 & Z_0 \\ 0 & 1 \end{pmatrix} , \tag{7}$$

$$[F_{hol}] = \begin{pmatrix} 1 & 0 \\ jB_{hol} & 1 \end{pmatrix} , \tag{8}$$

$$[F_{cav}] = \begin{pmatrix} 1 & Z_{cav} \\ 0 & 1 \end{pmatrix} , \tag{9}$$

$$[F_{wg}] = \begin{pmatrix} \cos\theta & jZ_0\sin\theta \\ j\sin\theta/Z_0 & \cos\theta \end{pmatrix} , \tag{10}$$

where $\theta = 2\pi\ell/\lambda_g$ and $\ell$ is the length of the waveguide. In the present system we adopt $\ell = 3\lambda_g/4$, where $\lambda_g = 6.97$ mm at $\omega_0/2\pi = 53.2$ GHz.

The voltage $E_\sigma$ and the current $I_\sigma$ at the input ($\sigma = i$) and the output ($\sigma = o$)

6

terminals [6] are related by

$$\begin{pmatrix} E_i \\ I_i \end{pmatrix} = \begin{pmatrix} A & B \\ C & D \end{pmatrix} \begin{pmatrix} E_o \\ I_o \end{pmatrix} . \tag{11}$$

The circuit, which consists of the power supply with the voltage $E_i$ and the load with $Z_0$, is expressed by the combination of elements with impedance $B/A$, power supply with the voltage of $E/A$ and the terminal load $Z_0$ as shown in Fig. 4. By using the maximum available power $P_{max} = |E_i|^2/4Z_0$, the power consumed by the terminal load $P_{out}$, transmission coefficient of the band rejection filter $T$ is calculated as

$$P_{out} = P_{max} T \tag{12}$$

$$T = \frac{4}{|B/Z_0 + A|^2} \tag{13}$$

The transmission coefficient $T$ depends on $A$ and $B$ of $F$-matrix elements as parameters of $Q_0$ and $n_R = n^2 R/Z_0 = Q_0/Q_E$.

The reflection coefficient $\Gamma$ is derived from Fig. 4 by $F$-matrix $[G]$

$$[G] = [F_{hol}][F_{cav}][F_{wg}][F_{hol}][F_{cav}][F_{wg}] \cdots \cdots$$

$$\cdots [F_{hol}][F_{cav}][F_{wg}][F_{hol}][F_{cav}][F_0] = \begin{pmatrix} A_G & B_G \\ C_G & D_G \end{pmatrix} \tag{14}$$

$$\Gamma = \left| \frac{Z_0 - B_G/D_G}{Z_0 + B_G/D_G} \right|^2 \tag{15}$$

Although $\lambda_g$ can be assumed to be constant near $\omega = \omega_0$ such as $|\Delta\omega/\omega_0| \le 0.0025$, in the wide range of 40~60 GHz, we take both dependencies of $\lambda_g$ on frequency and $jB_{hol}$ into consideration. The assumption of constant $\lambda_g$ results in the error within 0.01% for $53.2 \pm 0.133$ GHz.

The transmission and reflection coefficients in the system for any number of cavity are calculated as follows, for the assumption of constant $\lambda_g$ and $jB_{\text{hol}} = 0$.

$$
\left.
\begin{aligned}
T_1 &= \frac{4}{|y+2|^2}, \\[6pt]
T_2 &= \frac{4}{|y^2+2y+2|^2}, \\[6pt]
T_3 &= \frac{4}{|y^3+2y^2+3y+2|^2}, \\[6pt]
&\quad \dots\dots\dots\dots\dots\dots\dots\dots, \\[6pt]
T_{10} &= \frac{4}{|y^{10}+2y^9+10y^8+15y^7+35y^6+42y^5+50y^4+40y^3+25y^2+10y+2|^2},
\end{aligned}
\right\}
\tag{16}
$$

$$
\left.
\begin{aligned}
\Gamma_1 &= \frac{|y|^2}{|y+2|^2}, \\[6pt]
\Gamma_2 &= \frac{\left|y^2\right|^2}{|y^2+2y+2|^2}, \\[6pt]
\Gamma_3 &= \frac{\left|y^3+y\right|^2}{|y^3+2y^2+3y+2|^2}, \\[6pt]
&\quad \dots\dots\dots\dots\dots\dots\dots\dots, \\[6pt]
\Gamma_{10} &= \frac{\left|y^{10}+8y^8+21y^6+20y^4+5y^2\right|^2}{|y^{10}+2y^9+10y^8+15y^7+35y^6+42y^5+50y^4+40y^3+25y^2+10y+2|^2},
\end{aligned}
\right\}
\tag{17}
$$

where $y = Z_{\text{cav}}/Z_0$. The subscripts are the number of the cavities. In Figs. 5(a) and (b). the calculated results for $n_R = 0.50$, 1.0 and $Q_0 = 500$, 1000 are shown at $N = 5$ and 8, respectively. It is noted that the frequency-dependence and the rejection and the return loss at $\omega = \omega_0$ of the filter are determined by $Q_0$ and $n_R$ and that rejection increases proportionally with $N$.

# 3   Experimental procedures and results

We measure the insertion loss as a function of frequency. As a signal source the sweep generator is used and weak output signal as low as micro volt from the Schottky diode detector is observed by using the lock-in amplifier.

To compare the theoretical $n_R$ with the experimental one, we use single cavity filters

8

($N = 1$) with various $d$. With the aid of eq.(16), the best fitted $n_R$ is obtained from the frequency dependence such as Fig. 7 mentioned below. By $Q_E$ which is proportional to $d^{-6}$ given in Appendix I, the theoretical $n_R = Q_0/Q_E$ is derived. In Fig. 6, $n_R$ is plotted as a function of $d$. The experimental results show good agreement with the theoretical curve. Thus, we adopt $d \simeq 2.0 \pm 0.5$ mm for the present band rejection filter. To measure the rejection of the filter with $N = 10$ at first, each cavity in the band rejection filter is tuned so as to locate the center frequency of the attenuation at 53.2 GHz by scanning the frequency. The rejection characteristic for $N = 10$ is measured. Secondly, by inserting the plunger at the final cavity inward completely, performance of the band rejection filter with $N = 9$ is examined. By the same procedure, the next cavity is closed and the measurement for $N = 8$ is carried out. The Schottky diode detector is calibrated by the calibrated attenuator when all the cavities are closed. In Fig. 7, experimental results for the band rejection filter with the smallest coupling hole of $d = 1.6$ mm are plotted as a parameter of $N$. The attenuation (dB) is proportional to $N$ approximately. All the measured values for various $N$ agree fairly with the calculated curves by eq.(16) when $Q_0 = 700$ and $n_R = 0.20$ are assumed. The attenuation measurements for different coupling holes with $d = 2.0$ and 2.4 mm are carried out. In Fig. 8(a), rejections at $\omega = \omega_0$ are plotted as a function of $N$. Although the rejection for smallest coupling hole increases almost linearly, results from $d = 2.0$ and 2.4 mm increase nonlinearly. From the calculation with $jB_{\text{hol}} = 0$ described in the section 2, this nonlinear dependence of the attenuation on $N$ can not be expected. But this noticeable character can be explained by the mutual coupling ($jB_{\text{hol}} \neq 0$) between neighboring holes as discussed below. Practically, this enhancement of the attenuation is convenient in getting high attenuation at the center frequency.

In Fig.8(b) the experimental and the theoretical return loss (dB) from eq.(17) are shown as a function of $N$ for $d = 1.6$ mm. As predicted theoretically, with increasing $N$, return loss does not increase monotonously due to the increase in the absorption by the cavities but approaches fixed value after some oscillations by cancellations between scattered waves.

To study the nonlinear rejection for large coupling hole, three quarter-wavelength separated double cavity filter is used. At first, second cavity is closed and the frequency $\omega_{01}/2\pi$ at the maximum attenuation by the first one is tuned at 53.2 GHz. By decreasing the resonant frequency of second cavity $\omega_{02}/2\pi$ from 56 to 51 GHz with a step of 0.1 GHz by opening the second cavity, dependence of $\omega_{01}$ and attenuation in $\omega = \omega_{01}$ on $\omega_{02}$ with double-cavity system is estimated from the trough of attenuation by frequency scanning. Here, three rejection filters with the double cavity of which coupling hole is $d = 1.6$, 2.0 and 2.4 mm in diameter are experimentalized. Figures 9(a)~(c) show the frequency and the attenuation at the maximum attenuation corresponding to the first cavity from the measurement of frequency dependence for different $d$. Even if $\omega_{02}/2\pi$ decreases from 56 to 51 GHz in Figs. 9 (a), $\omega_{01}/2\pi$ of the first cavity does not change and attenuation increases as the superposition of rejection profiles. Here, the total attenuation is not additive and asymmetric profile at $\omega/2\pi = 53.2$ GHz is observed. As for $d = 2.0$ mm, when the second cavity is opened, $\omega_{01}/2\pi$ increases by 0.11 GHz. With decreasing $\omega_{02}/2\pi$, $\omega_{01}/2\pi$ reaches 53.2 GHz which is the initial value. The rejection becomes maximum at $\omega_{02}/2\pi = \omega_{01}/2\pi$ = 53.2 GHz. With reducing $\omega_{02}/2\pi$ from 53.2 GHz, $\omega_{01}/2\pi$ increases to 53.27 GHz. For the largest coupling hole of $d = 2.4$ mm as shown in Fig. 9(c), the shift of $\omega_{01}/2\pi$ is -0.10 GHz when the second cavity is just opened. With decreasing $\omega_{02}/2\pi$, $\omega_{01}/2\pi$ reaches the

minimum of 52.8 GHz and then increases up to 53.4 GHz. At the same time, the attenuation around $\omega/2\pi = 53.2$ GHz strongly increases. As a result of mutual coupling between cavities, the coupling coefficient $n_R$ increases and rejection rate is enhanced strongly in the multi-cavity system. The further study of the mechanism of the mutual coupling is left for the future.

# 4 Application of the band rejection filter

In Figs. 10(a) and (b), the attenuation and return loss of the band rejection filter with 10 cavities ($d = 2.0$ mm) in the whole frequency range for the second ECE measurement of 40~60 GHz are shown with the calculated result including finite $jB_{hol}$. In the calculation, parameters $n_R$ and $Q_0$ are selected as 1.2 and 1000 which are best values in fitting the experimental attenuation data around resonant frequency for $N = 10$ and $d = 2.0$ mm. In the heterodyne radiometer system for CHS, the filter with coupling holes of $d = 2.0$ mm is used from the viewpoint of attenuation level and the band width. The full width at half maximum (band width of the attenuation over 3 dB) at $\omega_0/2\pi = 53.2$ GHz is around 0.5 GHz and the rejection of 50 dB at $\omega_0/2\pi = 53.2$ GHz is obtained.

Experimental results show the peak around 40~45 GHz in Figs. 10(a) and (b). The exact calculation ($\theta \neq 3\pi/2$) including the frequency dependence of $\lambda_g$ in the waveguide between cavities by using eqs.(13), (15) and non-zero susceptance $jB_{hol} = j4\pi d^3 Y_0 \sin^2(x/a)/3\lambda_g a^2$ in $[F_{hol}]$ (see Appendix II) are shown in Figs. 10(a) and (b) as shown with solid curves. It is concluded that the peak at $\omega/2\pi = 40$~45 GHz, and many small peaks results manily from the mismatching between the waveguide and the coupling holes.

# 5  Conclusion

The band rejection filter is fabricated by using a series of three quarters-wavelength coupled cylindrical cavity with coupling hole installed in the waveguide. The obtained attenuation at 53.2 GHz is around 50 dB with the 3 dB bandwidth of 0.5 GHz for $N = 10$, $d = 2.0$ mm. By making the model which is represented by Tschebysheff polynomial with finite ohmic loss and the susceptance in the coupling hole, the comparison of the experiment with the model is performed and the good agreements are obtained. For the large diameter of coupling hole, it is confirmed experimentally that the strong mutual coupling between cavities exists. The developed band rejection filter satisfies the requirement from the ECE diagnostic system to eliminate the 53.2 GHz signal from a high-power millimeter source of the gyrotron for the purpose of plasma electron heating. From the experimental viewpoint, the size of holes and the number of cavity strongly affect observation because the emission from the plasma is very weak in comparison with the 53.2 GHz signal from the gyrotron. The optimum values of $d$ and $N$ are determined experimentally by taking the experimental requirements for ECE. In the present filter, the piston mechanism for adjusting the resonant frequency makes $Q_0$ low (theoretical value is four times larger than the experimental one). Full electrical contact by the contact finger in the gap and the fine tuning mechanism for adjusting the resonant frequency in the cavity is required for increasing $Q_0$.

# 6  Acknowledgments

# References

[1] H.J. Hartfuss, W VII-AS Team, *Proc. of 12th Int. Conf. on Infrared and Millimeter Waves* 1987 xxix+394, p360 (Cat. No.87CH2490-1).

[2] T. Geist, *Proc. of 8th Joint Workshop on Electron Cyclotron Emission and Electron Cyclotron Resonance Heating,* Gut Ising, Germany 1992, EC-8 Conf. Proc. **2**, p.417

[3] G.L. Ragan, *Microwave Transmission Circuits* (McGraw-Hill Book Company, Inc., New York, 1948), p.667, 704.

[4] C.G. Montgomery, *Technique of Microwave Measurements* (McGraw-Hill Book Company, Inc., New York, 1947), p.300, p.862, p.115, p.315.

[5] B. Oguchi, *Microwave and Millimeter Wave Circuit* ( Maruzen, Inc., 1964), p.148, p.286 [in Japanese].

[6] A.L.Pike, *Fundamentals of Electronic Circuits* (Prentice Hall, Inc., Engelewood Cliffs. New Jersey 1971), p.162.

# Appendix I (Calculation of the external $Q$)

Calculation of $Q_E$ for coupling of $TE_{10}$ mode in the rectangular waveguide with $TE_{11}$ circular mode in the cavity was reported [8]. Let consider the coupling of $TE_{10}$ mode in the rectangular waveguide with $TE_{111}$ mode in the cylindrical cavity by rf magnetic field. The Cartesian coordinate in the system is shown in Fig. I-1. The electromotive forces $E^+$ and $E^-$ for $+z$ and $-z$ directions are given by

$$E^{\pm} = \mp \left( h^* \pm h_z^* \right) \cdot J_{m0}, \qquad (I-1)$$

where $J_{m0}$ is the magnetic current in the cylindrical cavity and the subscription 0 means the value at the coupling hole. Here, $h^*$ is the complex conjugate of the $TE_{10}$ mode function of the rectangular waveguide with $a = 2b$ given by

$$h_{x0} = \frac{2}{a}\sin\frac{\pi x}{a}, \qquad (I-2a)$$

$$h_{y0} = 0, \qquad (I-2b)$$

$$h_{z0} = -j\frac{\lambda_g}{a^2}\cos\frac{\pi x}{a}, \qquad (I-2c)$$

where $a$ and $b$ is sizes (4.8 mm × 2.4 mm) of the waveguide. The value of $\lambda_g$ is 6.97 mm for $TE_{10}$ mode and $x/a$ is equal to 7/16 at the coupling hole. Because the value of $h_{z0}$ is assumed to be zero, only the $x$ component of $J_{m0}$ is considered.

15

The resonant magnetic fields of TE$_{111}$ mode in the cylindrical cavity normalized with the stored energy $W = 1$ is given by

$$H_r = j\frac{\lambda_0\chi_{11}}{l_{cav}D_{cav}\sqrt{\mu_0}}K_{11}J_1'\left(2\chi_{11}r/D_{cav}\right)\left\{\begin{array}{c}\cos\phi \\ \\ \sin\phi\end{array}\right\}\cos\frac{\pi\zeta}{l_{cav}}, \qquad (I-3a)$$

$$H_\phi = \mp j\frac{\lambda_0\chi_{11}}{l_{cav}D_{cav}r\sqrt{\mu_0}}K_{11}J_1\left(2\chi_{11}r/D_{cav}\right)\left\{\begin{array}{c}\sin\phi \\ \\ \cos\varphi\end{array}\right\}\cos\frac{\pi\zeta}{l_{cav}}, \qquad (I-3b)$$

$$K_{11} = \frac{2}{\sqrt{\pi}l_{cav}}\frac{1}{\sqrt{\chi_{11}^2 - 1}J_1\left(\chi_{11}\right)}, \qquad (I-3c)$$

where $\mu_0$ is the magnetic permeability and $\lambda_0$ satisfies eq.(2). The symbol ($r, o, \zeta$) is the cylindrical coordinate in the cavity and $l_{cav}$ is the length of the cavity.

The magnetic dipole currents $J_{m0\sigma} = j\omega_0\mu_0\alpha\hat{M}H_{\sigma0}$ ($\sigma = r, \phi$) at $\zeta = 0$ are obtained by

$$J_{m0r} = -\frac{4\alpha\hat{M}}{D_{cav}}\sqrt{\frac{\pi}{l_{cav}^3\epsilon_0}}\frac{\chi_{11}}{\sqrt{\chi_{11}^2 - 1}}\frac{J_1'\left(2\chi_{11}r/D_{cav}\right)}{J_1\left(\chi_{11}\right)}\left\{\begin{array}{c}\cos\phi \\ \\ \sin\phi\end{array}\right\}, \qquad (I-4a)$$

$$J_{m0\phi} = -\frac{4\alpha\hat{M}}{D_{cav}}\sqrt{\frac{\pi}{l_{cav}^3\epsilon_0}}\frac{\chi_{11}}{\sqrt{\chi_{11}^2 - 1}}\frac{J_1\left(2\chi_{11}r/D_{cav}\right)}{J_1\left(\chi_{11}\right)}\left\{\begin{array}{c}\sin\phi \\ \\ \cos\phi\end{array}\right\}, \qquad (I-4b)$$

where $\alpha$ is given by eq.(3)and $\hat{M} = d^3/6$ is the polarizability of magnetic dipole and $\epsilon_0$ is the dielectric constant in the free space. The value of $2r/D_{cav}$ is $0.3/4.0$. The power transmitted from the coupling hole derived from the magnetic current is expressed by $P_L^+$ $= |E^+|^2/2Z_v$, where $Z_v = (\lambda_g/\lambda)Z_0$. By substituting $\phi = 0$ in eqs. (I-4a) and (I-4b), we have $J_{m0r} = J_{m0x}$ and $J_{m0\phi} = J_{m0z}$. Thus, $Q_E$ is given by

$$Q_E = \frac{\omega_0 W}{2P_L^+} \propto d^{-6}. \qquad (I-5)$$

From eq.(I-5), the external $Q_E$ is estimated to be 7730.

# Appendix II (Derivation of Component in $[F_{\text{hol}}]$)

By taking the perturbation to waveguide due to the finite size of coupling hole. we improve an analysis of attenuation and return loss for wideband characteristics. The matrix elements in polarizability of the magnetic dipole $\hat{M}$ can be assumed to be $\hat{M}_{xx} \gg \hat{M}_{zz}$ due to the configuration of the hole as discussed in Appendix I. The scattering matrix $S_{11}$ [5] is calculated by mode function $h_{x0}$ in Appendix I;

$$S_{11} = -\frac{j\omega}{2}\frac{\mu_0 \hat{M}_{xx} h_{x0}}{Z_v}.$$

(II $-$ 1)

The value of $S_{11}$ is equivalent to the parallel susceptance $jB_{\text{hol}}$;

$$jB_{\text{hol}} = -2S_{11}Y_0 = j\frac{4\pi d^3 Y_0}{3\lambda_g a^2}\sin^2\frac{7\pi}{16},$$

(II $-$ 2)

where $x/a = 7/16$ is substituted in $h_{x0}$. The $F$-matrix by cavity hole is expressed as

$$[F_{\text{hol}}] = \begin{pmatrix} 1 & 0 \\ jB_{\text{hol}} & 1 \end{pmatrix}.$$

(II $-$ 3)

17

# Figure captions

Fig. 1: Schematic drawing of the band rejection filter developed.

Fig. 2: Configuration of cavity and its holes. The center of coupling hole is not on the axis of the cavity. The interval between cavities is 5.3 mm which is equal to $3\lambda_g/4$ at the frequency of 53.2 GHz.

Fig. 3(a): Equivalent circuit of band rejection filter which is three quarters-wavelength coupled resonant cavity ; an element $Z_0$ connected to the power supply represents the impedance of power supply. The resonant circuit is expressed by the capacitance $C/n^2$, the inductance $Ln^2$ and the resistance $Rn^2$, where $n$ is coupling coefficient corresponding to the turn ratio in transformer model. The susceptance $jB_{\mathrm{hol}}$ shows the scattering from the coupling hole.

Fig. 3(b): Distributed constant circuit for the band rejection filter. Here, $Z_0$ is the impedance of the generator and matched load ; $Z_{\mathrm{cav}}$ and $Z_{\mathrm{wg}}$ are the impedance of the resonant cavity and waveguide between cavities, respectively. The susceptance $jB_{\mathrm{hol}}$ shows the scattering from the coupling hole.

Fig. 4: The equivalent circuit including $F$-matrix. The upper (lower) figure shows the circuit for calculating the transmission coefficient (the return loss).

Fig. 5(a): Example of calculated attenuation for different $Q_0$ and $n_R$. Here. thick solid, thick dotted, thin solid and thin dotted curves shows the calculations for ( $n_R = 0.50$. $Q_0 = 1000$, $N = 5$), ($n_R = 0.50$, $Q_0 = 500$, $N = 5$), ($n_R = 1.00$, $Q_0 = 1000$, $N = 5$), and ( $n_R = 1.00$, $Q_0 = 1000$, $N = 8$) respectively. Calculations are carried out with the assumption

18

of the constant $\lambda_g$ and $jB_{\text{hol}} = 0$.

Fig. 5(b): Example of calculated the return loss with different $Q_0$ and $n_R$. Here, thick solid, thick dotted, thin solid and thin dotted curves show the calculations for ($n_R = 0.50$, $Q_0 = 1000$, $N = 5$), ($n_R = 0.50$, $Q_0 = 500$, $N = 5$), ($n_R = 1.00$, $Q_0 = 1000$, $N = 5$), and ($n_R = 1.00$, $Q_0 = 1000$, $N = 8$). The thin dotted curve is superposed on the thin solid curve. Calculations are carried out with the assumption of the constant $\lambda_g$ and $jB_{\text{hol}} = 0$.

Fig. 6: Comparison of the experimental $n_R$ with theoretical one. Solid circles show the value of $n_R$ obtained by fitting the experimental frequency dependence of the rejection for $N = 1$. The solid line shows the result from the theoretical calculation with dipole approximation from eq.(I-5).

Fig. 7: Measured and calculated rejection characteristics of the band rejection filter with $d = 1.6$ mm for various $N$. The curves are calculated from eq.(16) with $n_R = 0.2$, $Q_0 = 700$. Here, $\omega_0/2\pi = 53.2$ GHz. Calculations are carried out with the assumption of the constant $\lambda_g$ and $jB_{\text{hol}} = 0$.

Fig. 8(a): Attenuation as a function of $N$. For the large hole with $d = 2.0$ mm the curve increases nonlinearly.

Fig. 8(b): Return loss as a function of $N$. Solid circles are experimental data for $d = 1.6$ mm. The dashed line and open circles are theoretical calculation for same $d$ with $n_R = 0.2$, $Q_0 = 700$.

Fig. 9: In the rejection filter with double cavities, when $\omega_{02}/2\pi$ at the maximum of the

19

attenuation by the second cavity is changed, the attenuation ($\bullet$) and the frequency (o) $\omega_{01}/2\pi$ at the maximum of the attenuation by the first cavity. Figures (a), (b) and (c) are experimental results from $d = 1.6$, 2.0 and 2.4 mm.

Fig. 10(a): Calculated attenuation characteristics (solid line) with taking frequency dependence of $\lambda_g$ and susceptance of the coupling hole into account for full bandwidth of 40~60 GHz. The experimental results with $d = 2.0$ mm and $N = 10$ are plotted as open circles. The calculation conditions are $d = 2.0$ mm, $n_R = 1.2$ and $Q_0 = 1000$.

Fig. 10(b): Return loss by the band rejection filter. Open circles show experimental results of $d = 2.0$ mm and $N = 10$. The solid line shows the result of the theoretical calculation with taking account of the frequency dependence of $\lambda_g$ and susceptance of the coupling hole. The calculation conditions are $d = 2.0$ mm, $n_R = 1.2$ and $Q_0 = 1000$.

Fig. I-1: Radiant voltage from the dipole stimulated by the coupling hole of cavity.

tunnig screw

cavity

U-band
waveguide

coupling hole

front view                    side view

Fig. 1



coupling hole          cylindrical cavity

4.0mm                  2.0mm

4.8mm

x

y

0.3mm

2.4mm

5.3mm

U-band waveguide
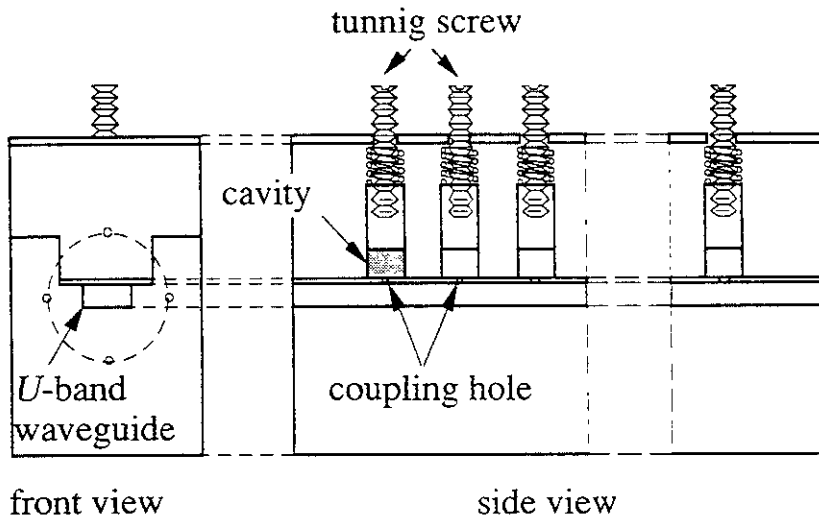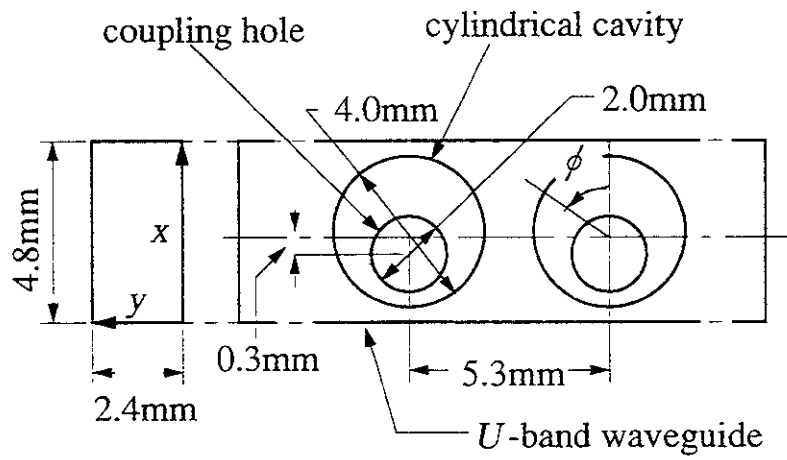
Fig. 2
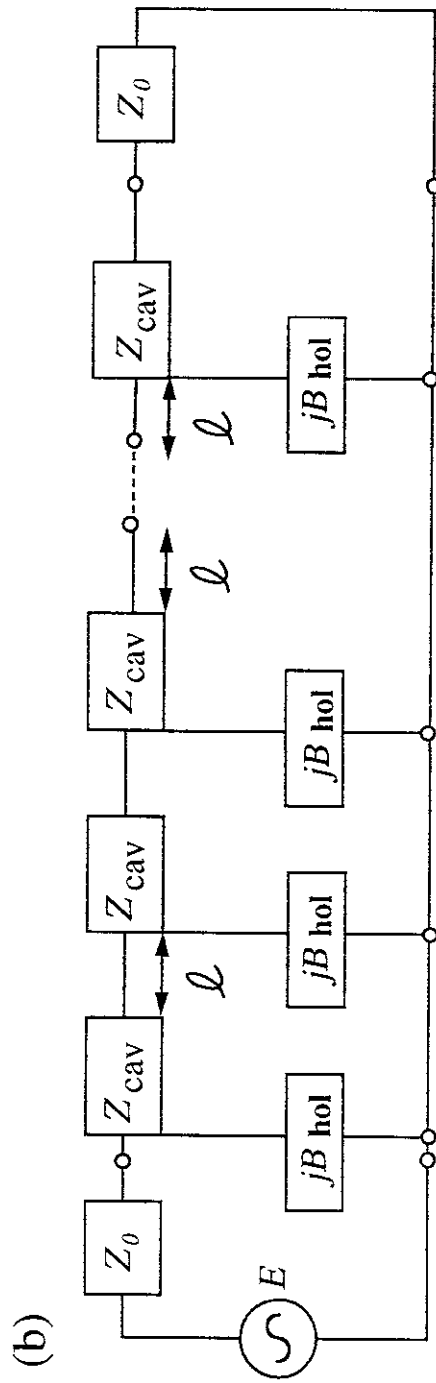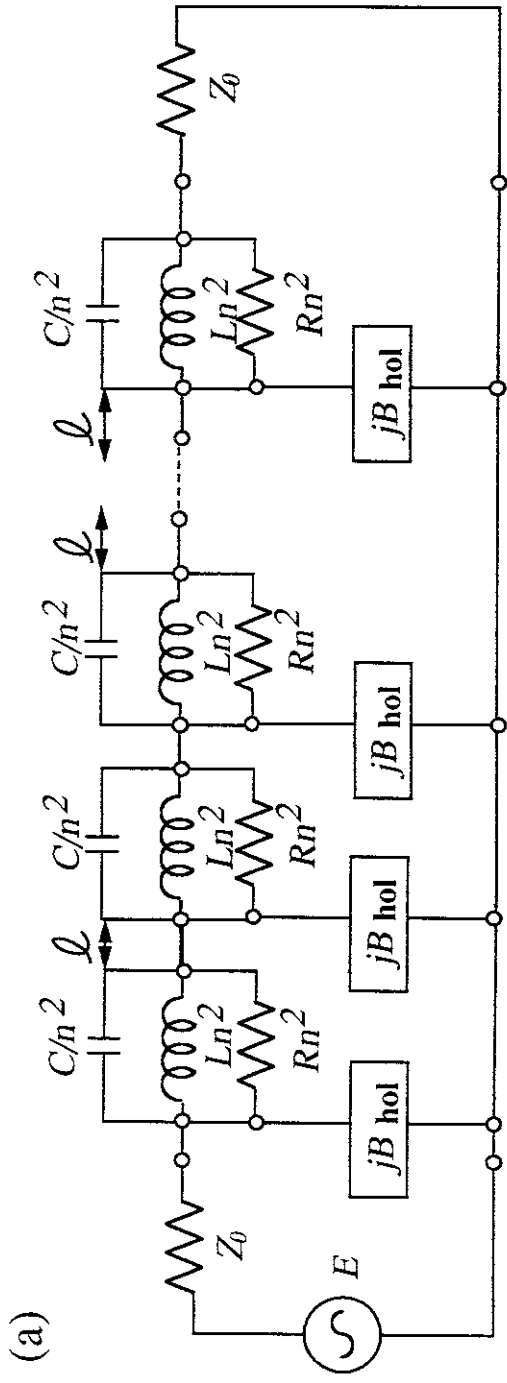
Fig. 3
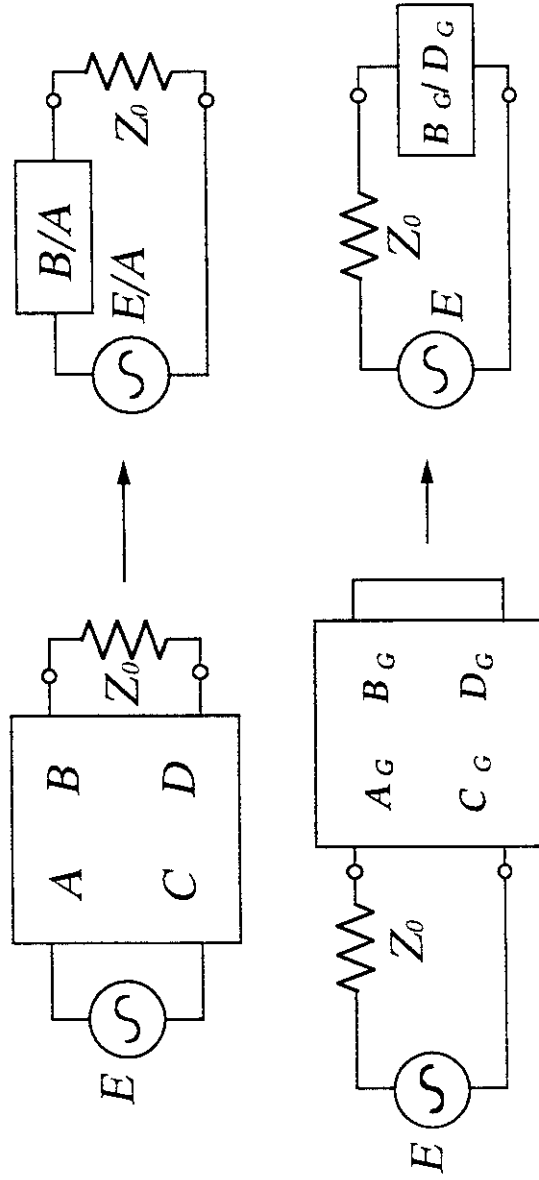
Fig. 4
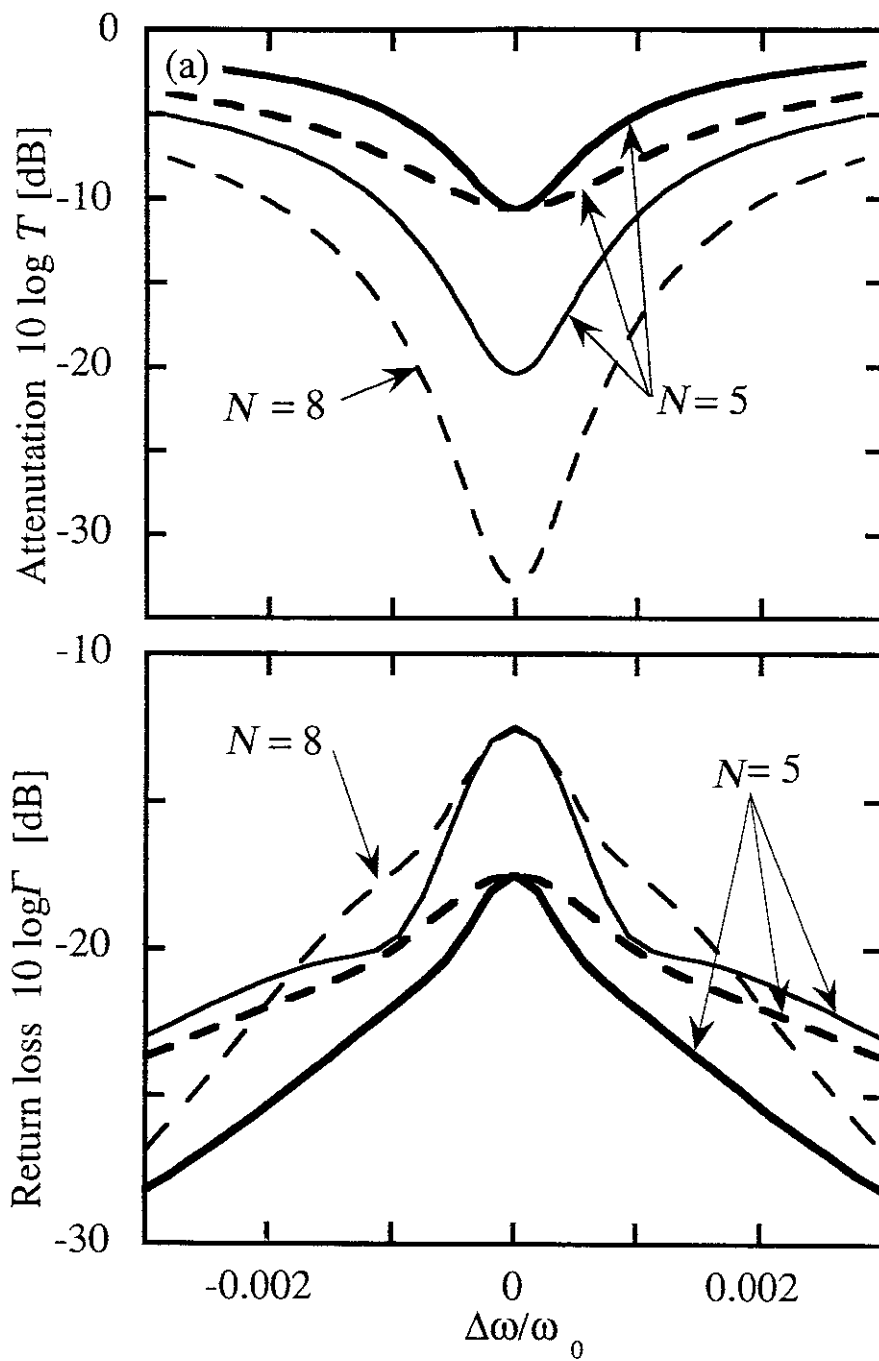
Fig. 5
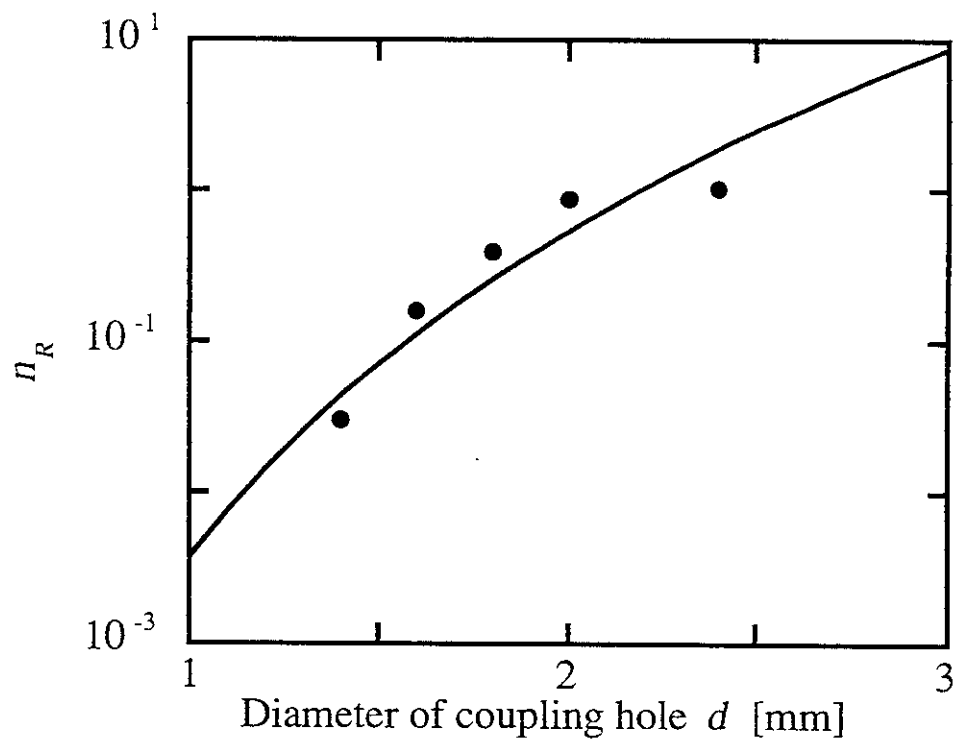
Fig. 6

Fig. 7

Fig. 8

Fig. 9

Fig. 10

cylindrical cavity

$E-$ ←      → $E+$

$U$-band waveguide          ← $x$

$z$ →

$y$
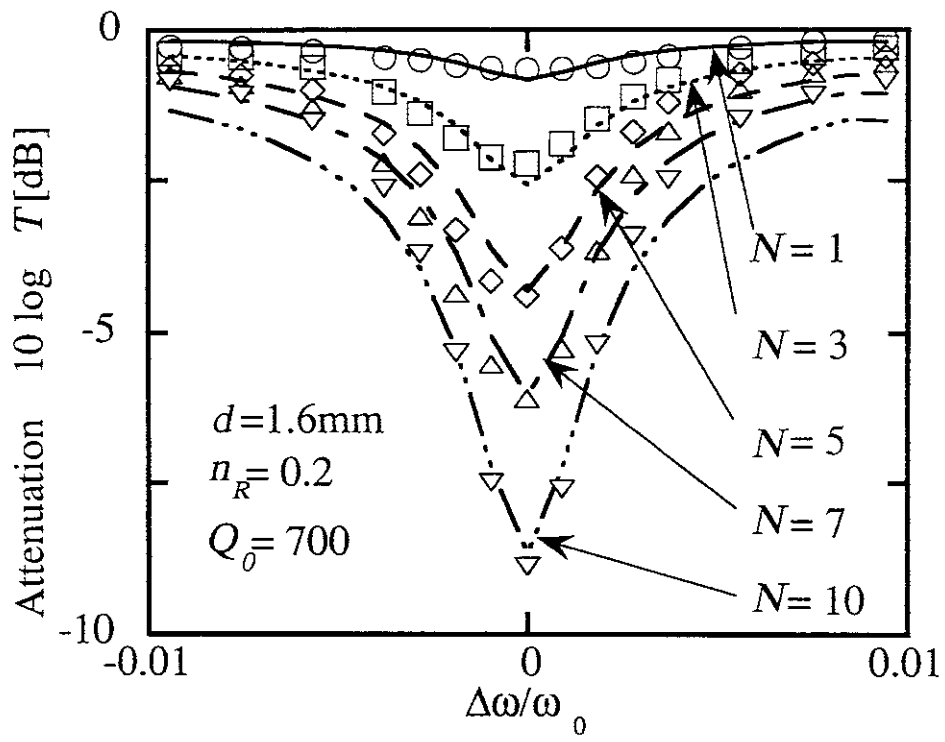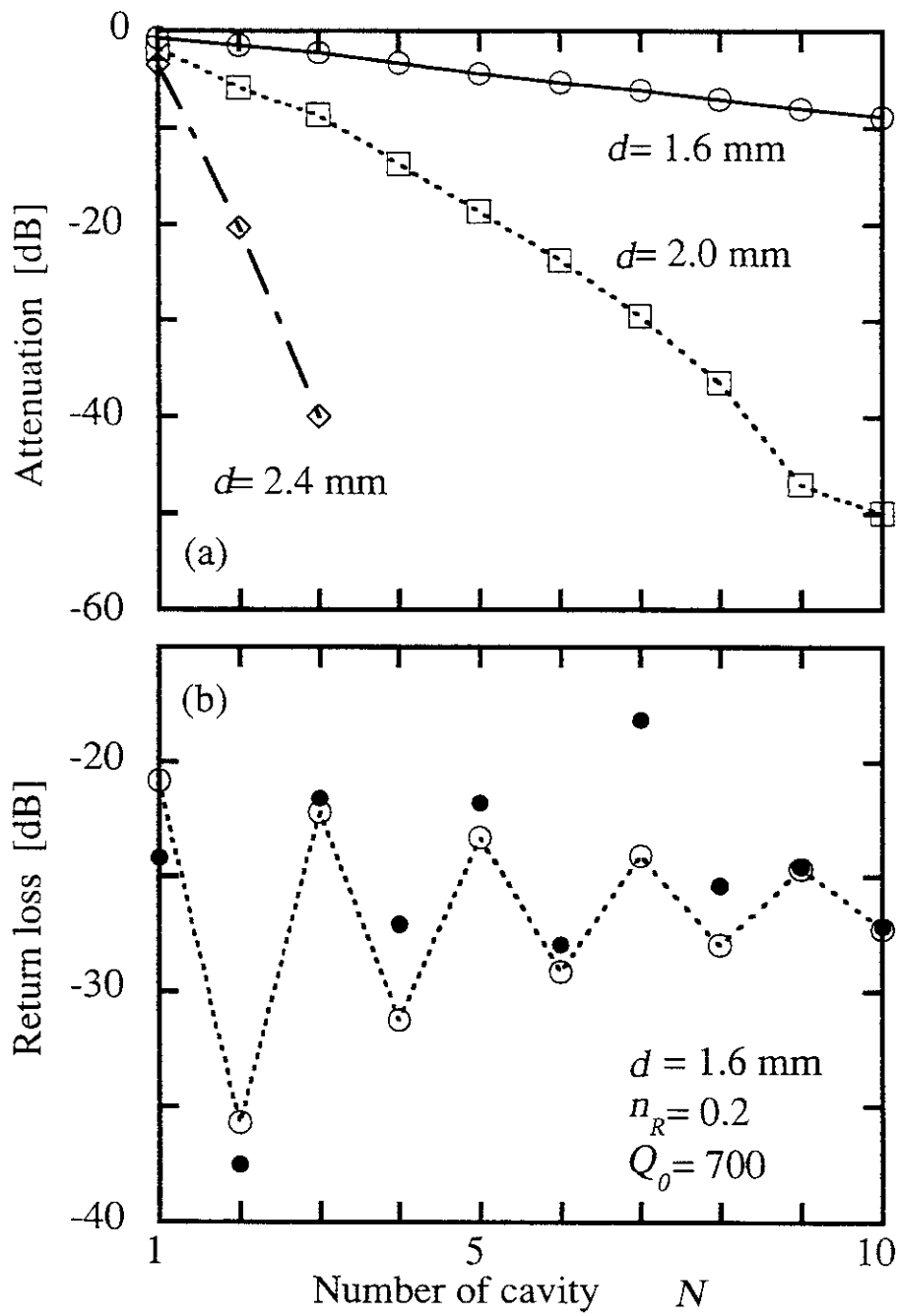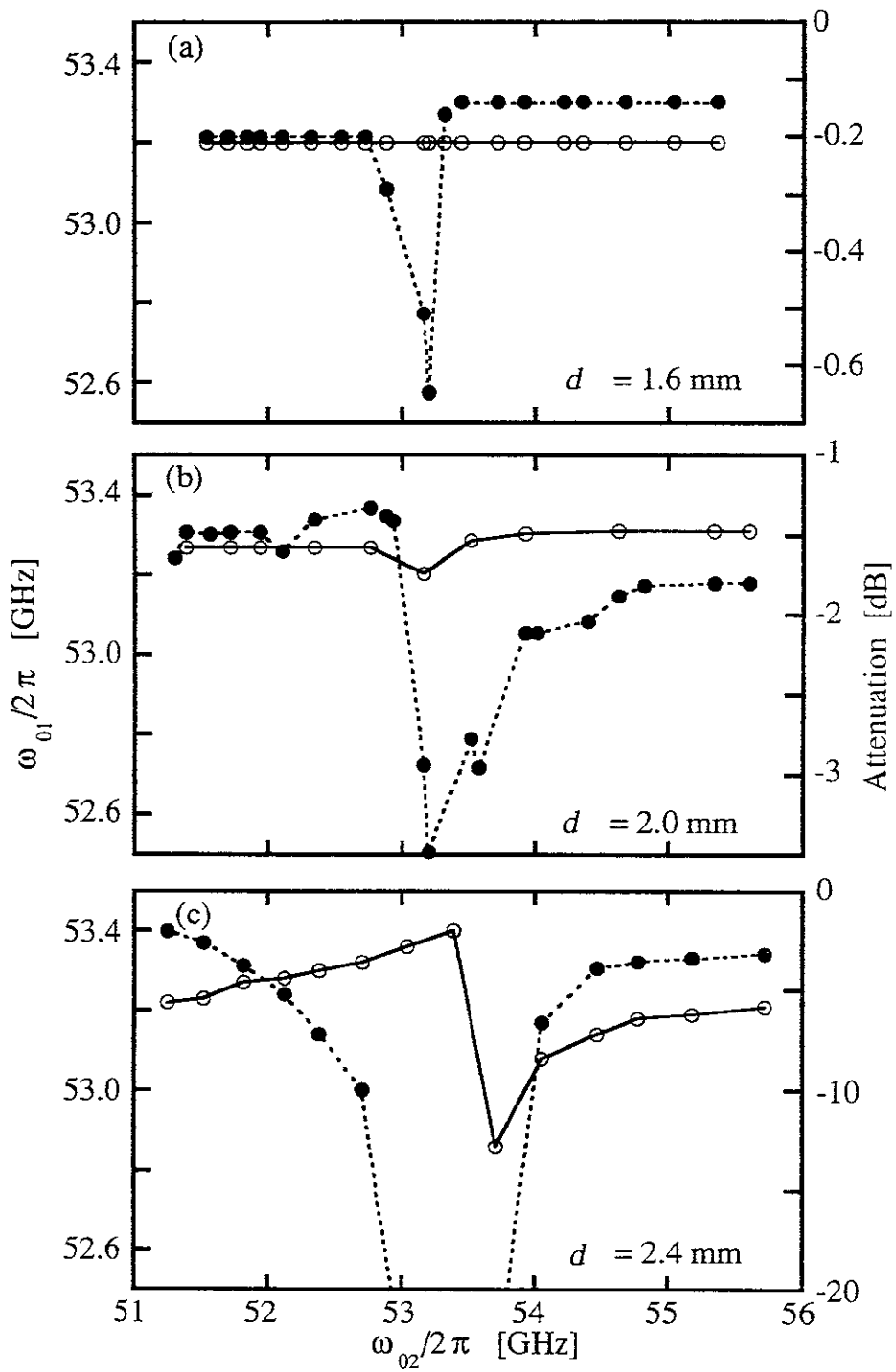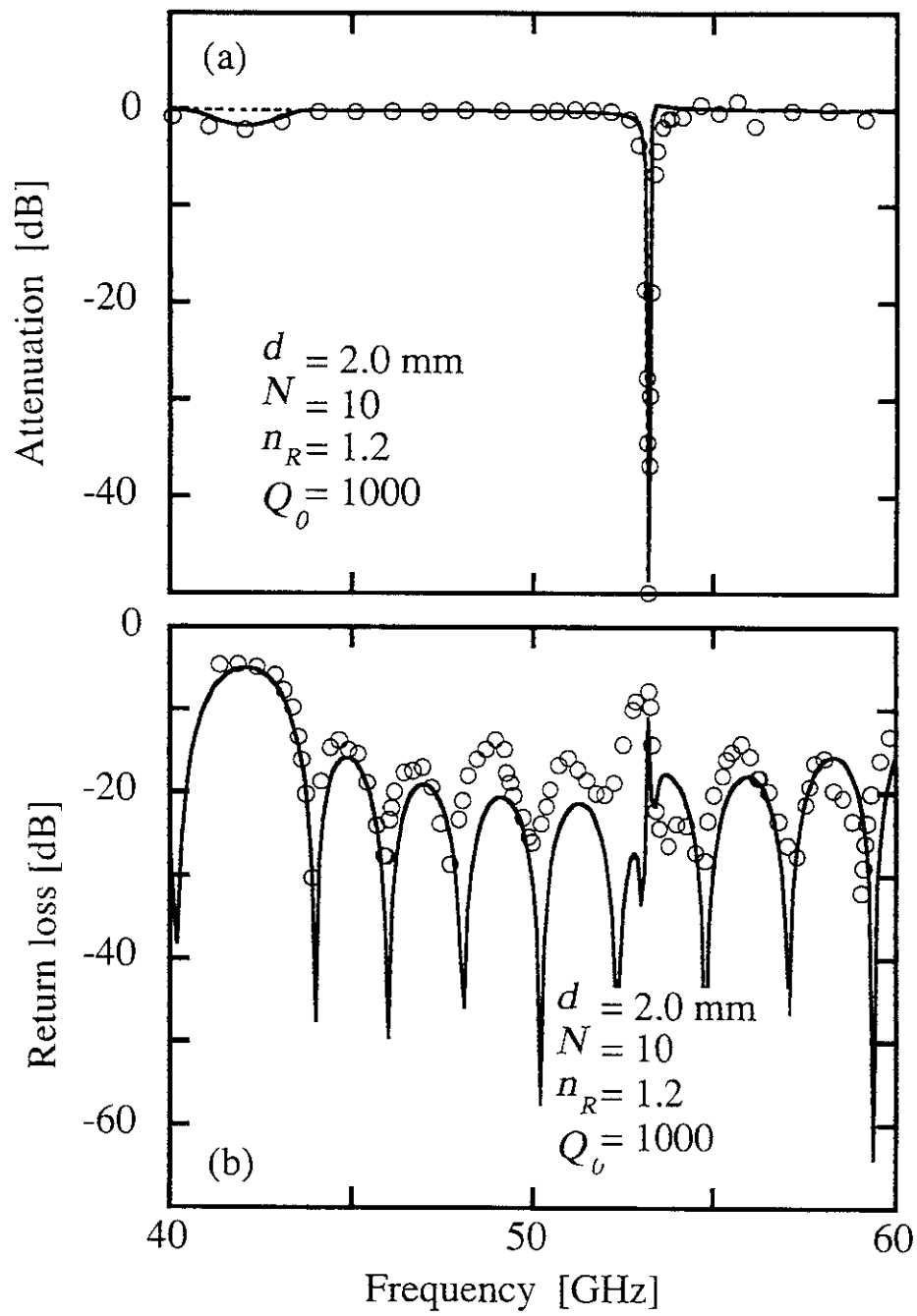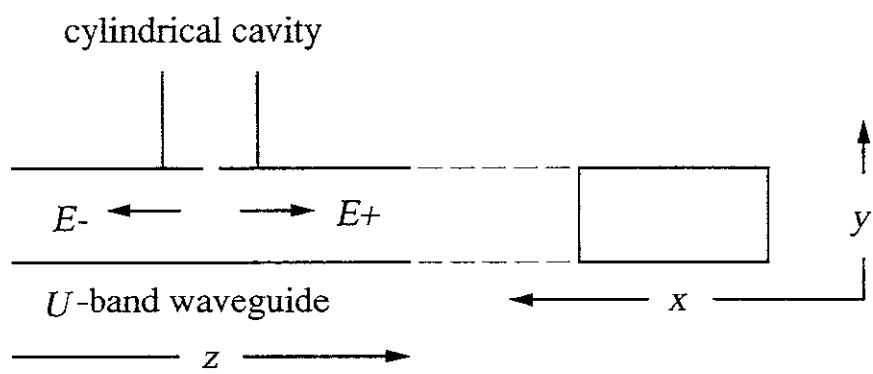
Fig.  I-1

# Recent Issues of NIFS Series

*Solitons;* Oct. 1995

NIFS-381 Y. Kondoh, M. Yoshizawa, A. Nakano and T. Yabe,
*Self-organization of Two-dimensional Incompressible Viscous Flow in a Friction-free Box;* Oct. 1995

NIFS-382 Y.N. Nejoh and H. Sanuki,
*The Effects of the Beam and Ion Temperatures on Ion-Acoustic Waves in an Electron Beam-Plasma System;* Oct. 1995

NIFS-383 K. Ichiguchi, O. Motojima, K. Yamazaki, N. Nakajima and M. Okamoto
*Flexibility of LHD Configuration with Multi-Layer Helical Coils;* Nov. 1995

NIFS-384 D. Biskamp, E. Schwarz and J.F. Drake,
*Two-dimensional Electron Magnetohydrodynamic Turbulence;* Nov. 1995

NIFS-385 H. Kitabata, T. Hayashi, T. Sato and Complexity Simulation Group,
*Impulsive Nature in Collisional Driven Reconnection;* Nov. 1995

NIFS-386 Y. Katoh, T. Muroga, A. Kohyama, R.E. Stoller, C. Namba and O. Motojima,
*Rate Theory Modeling of Defect Evolution under Cascade Damage Conditions:The Influence of Vacancy-type Cascade Remnants and Application to the Defect Production Chracterization by Microstructural Analysis;* Nov. 1995

NIFS-387 K. Araki, S. Yanase and J. Mizushima,
*Symmetry Breaking by Differential Rotation and Saddle-node Bifurcation of the Thermal Convection in a Spherical Shell;* Dec. 1995

NIFS-388 V.D. Pustovitov,
*Control of Pfirsch-Schlüter Current by External Poloidal Magnetic Field in Conventional Stellarators;* Dec. 1995

NIFS-389 K. Akaishi,
*On the Outgassing Rate Versus Time Characteristics in the Pump-down of an Unbaked Vacuum System;* Dec. 1995

NIFS-390 K.N. Sato, S. Murakami, N. Nakajima, K. Itoh,
*Possibility of Simulation Experiments for Fast Particle Physics in Large Helical Device (LHD);* Dec. 1995

NIFS-391 W.X.Wang, M. Okamoto, N. Nakajima, S. Murakami and N. Ohyabu,
*A Monte Carlo Simulation Model for the Steady-State Plasma in the Scrape-off Layer;* Dec. 1995

NIFS-392 Shao-ping Zhu, R. Horiuchi, T. Sato and The Complexity Simulation Group,
*Self-organization Process of a Magnetohydrodynamic Plasma in the*

*Presence of Thermal Conduction;* Dec. 1995

NIFS-393     M. Ozaki, T. Sato, R. Horiuchi and the Complexity Simulation Group
*Electromagnetic Instability and Anomalous Resistivity in a Magnetic Neutral Sheet;* Dec. 1995

NIFS-394     K. Itoh, S.-I Itoh, M. Yagi and A. Fukuyama,
*Subcritical Excitation of Plasma Turbulence;* Jan. 1996

NIFS-395     H. Sugama and M. Okamoto, W. Horton and M. Wakatani,
*Transport Processes and Entropy Production in Toroidal Plasmas with Gyrokinetic Eletromagnetic Turbulence;* Jan. 1996

NIFS-396     T. Kato, T. Fujiwara and Y. Hanaoka,
*X-ray Spectral Analysis of Yohkoh BCS Data on Sep. 6 1992 Flares - Blue Shift Component and Ion Abundances -;* Feb. 1996

NIFS-397     H. Kuramoto, N. Hiraki, S. Moriyama, K. Toi, K. Sato, K. Narihara, A. Ejiri, T. Seki and JIPP T-IIU Group,
*Measurement of the Poloidal Magnetic Field Profile with High Time Resolution Zeeman Polarimeter in the JIPP T-IIU Tokamak;* Feb. 1996

NIFS-398     J.F. Wang, T. Amano, Y. Ogawa, N. Inoue,
*Simulation of Burning Plasma Dynamics in ITER;* Feb. 1996

NIFS-399     K. Itoh, S-I. Itoh, A. Fukuyama and M. Yagi,
*Theory of Self-Sustained Turbulence in Confined Plasmas;* Feb. 1996

NIFS-400     J. Uramoto,
*A Detection Method of Negative Pionlike Particles from a H2 Gas Descharge Plasma;* Feb. 1996

NIFS-401     K.Ida, J.Xu, K.N.Sato, H.Sakakita and JIPP TII-U group,
*Fast Charge Exchange Spectroscopy Using a Fabry-Perot Spectrometer in the JIPP TII-U Tokamak;* Feb. 1996

NIFS-402     T. Amano,
*Passive Shut-Down of ITER Plasma by Be Evaporation;* Feb. 1996

NIFS-403     K. Orito,
*A New Variable Transformation Technique for the Nonlinear Drift Vortex;* Feb. 1996

NIFS-404     T. Oike, K. Kitachi, S. Ohdachi, K. Toi, S. Sakakibara, S. Morita, T. Morisaki, H. Suzuki, S. Okamura, K. Matsuoka and CHS group;
*Measurement of Magnetic Field Fluctuations near Plasma Edge with Movable Magnetic Probe Array in the CHS Heliotron/Torsatron;* Mar. 1996

NIFS-405    S.K. Guharay, K. Tsumori, M. Hamabe, Y. Takeiri, O. Kaneko, T. Kuroda,
            *Simple Emittance Measurement of H- Beams from a Large Plasma Source*; Mar. 1996

NIFS-406    M. Tanaka and D. Biskamp,
            *Symmetry-Breaking due to Parallel Electron Motion and Resultant Scaling in Collisionless Magnetic Reconnection*; Mar. 1996

NIFS-407    K. Kitachi, T. Oike, S. Ohdachi, K. Toi, R. Akiyama, A. Ejiri, Y. Hamada,
            H.Kuramoto, K. Narihara, T. Seki and JIPP T-IIU Group,
            *Measurement of Magnetic Field Fluctuations within Last Closed Flux Surface with Movable Magnetic Probe Array in the JIPP T-IIU Tokamak*;
            Mar. 1996

NIFS-408    K. Hirose, S. Saito and Yoshi.H. Ichikawa
            *Structure of Period-2 Step-1 Accelerator Island in Area Preserving Maps*;
            Mar. 1996

NIFS-409    G.Y.Yu, M. Okamoto, H. Sanuki, T. Amano,
            *Effect of Plasma Inertia on Vertical Displacement Instability in Tokamaks*; Mar. 1996

NIFS-410    T. Yamagishi,
            *Solution of Initial Value Problem of Gyro-Kinetic Equation*; Mar. 1996

NIFS-411    K. Ida and N. Nakajima,
            *Comparison of Parallel Viscosity with Neoclassical Theory*; Apr. 1996

NIFS-412    T. Ohkawa and H. Ohkawa,
            *Cuspher, A Combined Confinement System*; Apr. 1996

NIFS-413    Y. Nomura, Y.H. Ichikawa and A.T. Filippov,
            *Stochasticity in the Josephson Map*; Apr. 1996

NIFS-414    J. Uramoto,
            *Production Mechanism of Negative Pionlike Particles in $H_2$ Gas Discharge Plasma*; Apr. 1996

NIFS-415    A. Fujisawa, H. Iguchi, S. Lee, T.P. Crowley, Y. Hamada, S. Hidekuma, M. Kojima,
            *Active Trajectory Control for a Heavy Ion Beam Probe on the Compact Helical System*; May 1996

NIFS-416    M. Iwase, K. Ohkubo, S. Kubo and H. Idei
            *Band Rejection Filter for Measurement of Electron Cyclotron Emission during Electron Cyclotron Heating*; May 1996